Crimson Publishers
Wings to the Research

Research Article

Mineralogical Characterization of Tailings by using Hyperspectral Techniques and its Application in Predicting Rheological Properties

ISSN: 2578-0255

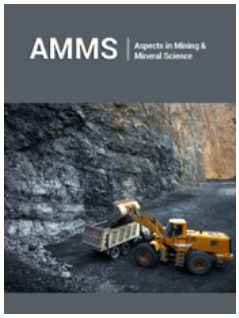

Voisin Leandro[1,2]*, Urrutia Nicolás[2] and Ossandon Julio[3]

[1]DIMIN, Mining Engineering Department, University of Chile, Chile

[2]AMTC, Advanced Mining Technology Center, University of Chile, Chile

[3]ENAMI, Mining Development Agency of Chile, Chile

***Corresponding author:** Voisin Leandro, DIMIN, Mining Engineering Department, University of Chile, 2069 Tupper Avenue, Santiago, Chile

Submission: October 01, 2024
Published: November 07, 2024

Volume 12 - Issue 5

How to cite this article: Voisin Leandro*, Urrutia Nicolás and Ossandon Julio. Mineralogical Characterization of Tailings by using Hyperspectral Techniques and its Application in Predicting Rheological Properties. Aspects Min Miner Sci. 12(5). AMMS. 000797. 2024.
DOI: 10.31031/AMMS.2024.12.000797

Abstract

Advanced mineral characterization techniques play a crucial role in the mining industry, particularly in predicting and controlling the rheological behavior of suspensions such as mineral pulps, concentrates, and tailings. For the latter, the ability to accurately assess mineral composition, especially the presence of phyllosilicates, is essential for understanding the challenges associated with tailings transport and disposal, which pose significant long-term risks. Previous studies have shown that solid content by volume, particle size, and mineralogy are the main factors influencing tailings rheology. This study aims to quantify the effects of these properties, with a specific focus on the influence of some phyllosilicates, on the viscosity (η) and yield stress (τ) of tailings. Techniques such as hyperspectral, XRF, XRD, and laser diffraction particle size analysis were assessed as tools for supporting predictive control of tailings mineralogy and rheology. A total of 108 tailings mixtures were adjusted by blending Chilean copper mine tailings with kaolinite and montmorillonite, varying factors such as solids content by volume (ϕ), particle size (d_{80}), phyllosilicate content in the solid phase ($wt\%_{phy}$), and the type of phyllosilicate (phy. type) to generate flow curves.

Two linear regression models were applied to predict viscosity and yield stress, with the logarithmic model yielding the best results (R^2=0.98 for Log(τ) and 0.96 for Log(η)). These models were validated using phyllosilicate abundance data from reflectance spectroscopy measurements on briquettes with the same composition as the experimental samples. While kaolinite content was underestimated and montmorillonite overestimated, leading to an overestimation of η and τ at higher values, the findings confirm that the key variables effectively estimate viscosity and yield stress. This supports the potential for implementing predictive control systems using advanced mineral characterization techniques.

Keywords: Advanced characterization; Phyllosilicate; Tailings; Geometallurgy; Reflectance spectroscopy

Introduction

Tailings transport and disposal are critical concerns in the mining industry due to their environmental impact and long-term risks, such as reagent-laden water percolating into soils and the potential for large-scale mudslides. Additionally, transporting tailings through mine and plant circuits via pumping systems can encounter disruptions and failures caused by significant changes in the rheology of the pulp. The rheological behavior of suspensions, particularly the influence of phyllosilicates on viscosity and yield stress, has been extensively studied [1-8]. However, only a few mathematical models based on mineral characterization have been developed [9,10], making the creation of an empirical model useful for predicting the rheological behavior of pulps, tailings, and other metallurgical phases. Such a model would assist in the design and operation of pipelines and pumps.

This study aims to develop an empirical model to estimate the viscosity and yield stress of tailings containing phyllosilicates (montmorillonite and kaolinite) based on the use of data obtained from advanced characterization techniques, such as quantitative XRD, laser diffraction particle size analysis, and hyper spectrometry. For the latter, reflectance data was obtained by using Hylogger3 technology and analyzed using The Spectral Geologist Software (TSG™) [11] and incorporated into the model, which was then compared with the rheological measurements of the samples.

Theoretical Considerations

Rheological properties of suspensions

Several authors have studied the effect of different variables on suspension rheology [2,7,12-18]. According to the literature, the most significant factors are: 1) solids content by volume, 2) particle size and shape, 3) the presence of phyllosilicates, and 4) the reagents used. The behavior of suspensions as a function of solids content by volume (ϕ) is well documented [16,17,19]. As ϕ increases, both viscosity and yield stress rise, eventually reaching a point where even a small increase in ϕ can lead to dramatic changes in these properties, a pattern confirmed by studies conducted on various Southern African platinum ores [2].

Various mineral species (e.g., phyllosilicates) tend to appear almost exclusively in specific particle shapes. Minerals with rod-like or plate-like shapes exert a greater influence on viscosity and yield stress than those with granular or spherical forms [19]. Consequently, an increase in certain mineral types, such as phyllosilicates, within the solid phase tends to elevate both viscosity and yield stress in suspensions [15]. Additionally, swelling clays typically exhibit increases in these rheological properties [2,14]. This swelling phenomenon originates from the charge anisotropy inherent in phyllosilicate minerals, which leads to two distinct swelling mechanisms: (1) inter-crystalline expansion and (2) osmotic expansion [20]. Particle size is also a critical factor in suspension rheology, as smaller particles are more susceptible to external forces (e.g., DLVO forces-Derjaguin, Landau, Verwey, and Overbeek-, Brownian motion, and viscous forces) than to fluid movement itself, resulting in increased viscosity and yield stress. Previous studies have reported very conclusive findings on this topic [2,17].

Hylogger 3TH reflectance spectroscopy

The Hylogger3 is a semi-automated device designed for the rapid collection of high-density spectral reflectance measurements in the visible-near infrared (VNIR; 350-1000nm), shortwave infrared (SWIR; 1000-2500nm), and thermal infrared (TIR; 6000 to 14500nm) regions, along with continuous high-resolution color imagery of samples in a non-invasive, non-destructive manner. Different wavelength regions are sensitive to different minerals [21]. For instance, iron oxides can be detected in the VNIR range, while phyllosilicates and other alteration minerals, such as carbonates, jarosites, micas, alunites, pyrophyllite, and chlorites, are active in the SWIR range. The TIR is particularly suitable for detecting nominally anhydrous silicates (e.g., quartz, olivines, and pyroxenes) as well as borates, sulfates, and carbonates.

Acquiring reflectance spectra from fine-grained material, such as tailings, is challenging due to the influence of grain size on both the background and the intensity of absorption features. For example, decreasing grain size increases the reflectance values of phyllosilicates in the SWIR [22,23]. To minimize the effects of grain size on infrared reflectance spectra, samples can be pressed into briquettes. Additionally, samples must be scanned in a dry condition to reduce the impact of water-related absorption features. Hyperspectral data collected by the Hylogger3 is analyzed using the TSG™ software, specially developed by CSIRO for this purpose [11].

Samples and Mineral Characterization Methods

Samples and characterization

Copper mine tailings generated by different mineral processing plants located in Chile were used as samples for the experiments and characterization, as well as high-purity kaolinite and montmorillonite as doping components for those samples, both phyllosilicates provided by Sigma-Aldrich Co. The solids were suspended in demineralized distilled water, and a NaOH (produced by Merck KGaA) 16M solution was used as a pH regulator in the montmorillonite-bearing samples. Mineral characterization of the tailings, kaolinite, and montmorillonite was conducted through XRD analysis (diffractometer, D8 Advance model, designed by Bruker in Germany) and reflectance spectroscopy measurements (HyLogger3, developed by CSIRO in Australia). The particle size distribution of the materials was measured using laser diffraction (Mastersizer 2000 model, Malvern Panalytical, UK). This technique analyzes light scattering patterns as particles pass through a laser beam, allowing for accurate determination of particle size distribution. The method is particularly suitable for phyllosilicates, which contain a significant proportion of particles below 38μm (-400# ASTM).

For density measurements, a 100ml volumetric flask was first weighed, partially filled with approximately 1cm of solids, and the total weight was recorded. Then, 30ml of distilled water was added to the solids, and the mixture was subjected to a vacuum to remove any residual air bubbles trapped within the solid phase. Once bubbling ceased, the flask was filled with distilled water to reach a total volume of 100ml and weighed again. The density of distilled water was determined by filling the same flask with water and measuring its volume and mass. The humidity content of montmorillonite and kaolinite was determined using the following procedure: 1) weighing the mineral sample, 2) drying it at 120 °C for 24 hours, and 3) weighing the dry sample. To verify the results, the dry sample was left exposed to room temperature conditions and weighed again, allowing it to regain its natural humidity and achieve nearly the same original mass.

Preparation of suspensions

The tailings were dried and sieved into the size categories listed in Table 1, following ASTM E11-17 standard guidelines, which

specify precise sieve mesh sizes for particle size analysis. Each fraction was stored for suspension (pulp) preparation, except for the +100# ASTM fraction, which was discarded to prevent potential issues with the rheometer due to the limited space between the cylinder and the cup. For the -400# ASTM fraction, the material was washed through a -400# ASTM sieve, ensuring compliance with ASTM procedures for fine particles, then dried and re-sieved to avoid contamination with other fine fractions. A total of 108 suspensions were prepared: 48 containing tailings dopped with kaolinite, 48 containing tailings dopped with montmorillonite, and 12 without phyllosilicates doping, the latter were used as baseline measurements. For each phyllosilicate, three solid contents were prepared (25, 30, and 40 vol%), with four particle size distributions (d_{80} values of 86.43, 73.99, 63.94, and 43.79μm), and four phyllosilicate contents in the solid phase (5, 10, 15, and 25 wt%).

Table 1: Sieves used in tailings classification.

Particle size, μm	ASTM Mesh
150	100
106	140
75	200
53	270
45	325
38	400

To maintain a consistent particle size distribution for each set of experiments with the same d_{80} values, specific amounts of the tailings' particle size fractions were added. The solid phase of the pulp was thoroughly mixed and then combined with distilled water in a 250ml Erlenmeyer flask. To ensure proper mixing of all phases, the flasks were agitated in a WiseCube WIS-20 shaking incubator (model WIS-20, manufactured by Witeg, Germany) at 250rpm (room temperature) for one hour. The experiments were carried out at a neutral pH of 7. Suspensions containing tailings and kaolinite did not require pH adjustment, as their natural range was from 6.8 to 7. In contrast, suspensions with tailings and montmorillonite initially reported a pH of 2, necessitating the addition of 16M and 8M NaOH solutions for coarse and fine pH adjustments, respectively. Buffer solutions were not used to avoid the formation of additional compounds (due to the presence of salts) that could alter the composition and rheological behavior of the pulps.

Rheology measurements

The rheometries were conducted using a rheometer (model RheolabQC®, manufactured by Anton Paar, Graz, Austria) equipped with a CC-39 measuring system (concentric cylinder), equipped with a CC-39 measuring system (concentric cylinder), as shown in Figure 1. Standard flow curves (shear stress vs. shear rate) were obtained by linearly increasing the shear rate from 0 to $300s^{-1}$ over a period of 60 seconds, recording 200 data points (one point every 0.3 seconds). The selection of this shear rate range was based on preliminary tests conducted with the same materials and rheometer in the laboratory. These tests indicated that some samples exhibit shear-thickening behavior at shear rates above $200s^{-1}$, likely due to the generation of random flows within the measuring system. This transition point shifts to higher shear rate values as the viscosity of the measured pulp increases. The procedure started when the pulp sample was removed from the shaking incubator and, if necessary, underwent pH adjustment. During this stage, the sample was manually agitated to ensure homogeneity. The pulp was then transferred into the rheometer's measuring cup, and the rheometric test was initiated. After each test, all components of the system were thoroughly cleaned with distilled water to remove any residual material.

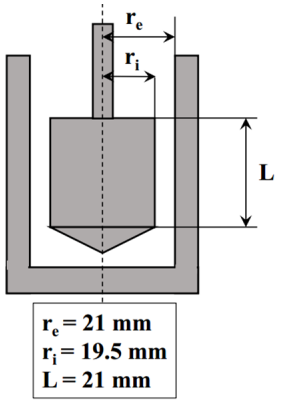

Figure 1: CC39 Measuring system dimensions.

Preparation of tailing briquettes

Water contained in samples has characteristic absorption features at 1400nm and 1900nm, the latter being a key feature of certain minerals such as montmorillonite. Additionally, previous measurements related to this study indicated that the analysis results from Hylogger3 are more reliable when the powder has been compacted prior to scanning. Based on these considerations, dry briquettes were prepared with the same solid composition as the suspensions used in the rheometric experiments. The briquettes were formed by applying a load equivalent to 6 metric tons using a hydraulic press, resulting in cylindrical samples measuring 3cm in diameter and 2cm in height. Given the various solid-phase compositions used in the pulps, 36 briquettes were prepared: 32 containing tailings with phyllosilicates (four d_{80} values, four phyllosilicate contents in the solid phase, and two types of phyllosilicates) and four briquettes of tailings without the addition of phyllosilicates (four d_{80} values). Additionally, one briquette of each pure phyllosilicate was prepared, bringing the total to 38 briquettes, which were stored in opaque, dark trays for scanning with the Hylogger3.

Empirical model development

The Bingham plastic model was fitted to the measured flow curves to predict their behavior at shear rates higher than $300s^{-1}$, though it lacks precision at low shear rates. From this model, two key parameters were obtained for each measurement: Bingham yield stress (τ_B) and Bingham viscosity (η_B). Both parameters were independently used to perform linear regressions, aiming to correlate them with the solid content by volume ("ϕ"), particle

size distribution ("d_{80}"), phyllosilicate content in the solid phase ("$wt\%_{phy}$"), and the type of phyllosilicate ("phy. type") used in the experiments.

Two different approaches were used for the linear regression. The first one, referred to as the "normal" method, directly predicted τ_B and η_B using ϕ, d_{80}, $wt\%_{phy}$, and phyllosilicate type as input variables. The second approach, known as the "logarithmic" method, predicted $Log(\tau_B)$ and $Log(\eta_B)$ using the same set of input variables. Phyllosilicate type was treated as a categorical variable, with kaolinite assigned a value of 1, montmorillonite assigned a value of 2, and the baseline (briquettes without phyllosilicates) assigned a value of 0.

Determination of model variables using SWIR reflectance spectra

Once briquettes were scanned using HyLogger3, spectral data was processed to obtain values for ϕ, d_{80}, $wt\%_{phy}$, and phyllosilicate type of each one of them. Since scanning was performed on solid dry briquettes, it is not possible to extract solids content by volume (ϕ) values from reflectance spectra. Additionally, the possibility to obtain information about particle size (d_{80}) through reflectance spectra was assessed. The presence and type of phyllosilicate values were extracted from SWIR reflectance spectra as described in coming sections 3.6.1 and 3.6.2.

Phyllosilicates differentiation: The "Phyllosilicate type" variable values were fixed by using scalars (mathematical functions of measured spectra) that specify which phyllosilicate is present in samples. For montmorillonite, the depths of 1900 and 2200nm features must be higher than 0.035 and 0.031 respectively, to ensure detection of Al-smectites specifically. In addition, the depth of the 2168nm feature needs to be lower than 0.1 to discard any kaolinite presence since it is a key feature of this phyllosilicate.

Kaolinite presence was determined by two rules: (1) the 2168nm feature depth must be higher than 0.002 and (2) the sum of depths of 2168 and 2208nm features need to be higher than 0.5. The first rule aims to a key spectral feature of kaolinite, while the second is used to ensure it has a presence equal to or greater than 5wt%.

Phyllosilicate quantification: Hyperspectral data collected from the samples scanning was processed to determine kaolinite and montmorillonite abundance, for that purpose two scalars were created, based on spectral references of these two minerals and the spectral data obtained from pure phyllosilicate briquettes.

Some of the phyllosilicates spectral features were assessed as potentially useful to generate abundance scalars. For kaolinite, the double feature at 2160 and 2220nm is very indicative of its presence (Frost & Johannson, 1998). It should be noted that absorption features at around 2160nm are also described from other minerals present in copper tailings, such as carbonates, hydroxyl-bearing sulphates, and pyrophyllite.

The "Kaolinite Index" (KI) scalar was built for every analyzed sample, where the depth of the 2160nm feature in each sample was divided by the depth of the 2160nm feature in pure phyllosilicate as a reference sample. Then, to calibrate the KI scalar, the average value of this scalar from samples containing 25 wt% of kaolinite was used as a calibration point, which is presented in Equation 1. Subsequently, the "Kaolinite Adjusted Index" (KAI) was obtained for each content of clays using the same adjustment coefficient.

$$KAI = \frac{25\%}{mean\ KI\ for\ 25\,wt\%\,kaolinite\,samples} \cdot KI \quad (1)$$

Montmorillonite scalar was created based on the 1900nm spectral feature, present in all hydrous minerals and even in some anhydrous ones which contain fluid inclusions, therefore, using this feature solely can lead to montmorillonite contents overestimation. To avoid problems the 2200nm feature must be considered since it is used as an indicator for Al-smectites presence. To confirm montmorillonite presence, the 2200nm feature needs to have minimum trough depth of 0.031. In addition, 1900nm feature asymmetry resulted useful for quantification, where lower values are related to higher contents of this phyllosilicate.

The "Montmorillonite Index" (MI) was created in four steps: (1) dividing 1900nm trough depth of every sample by the 1900nm trough depth of pure montmorillonite briquette, obtaining a normalized 1900nm depth; (2) normalizing 1900nm trough asymmetry of each sample by using the asymmetry value of this feature in pure montmorillonite briquette; (3) dividing normalized 1900nm depth by the normalized 1900nm asymmetry, and (4) multiplying the latter result by 1 if 2200nm trough depth is greater than 0.031, otherwise by 0. The adjustment of MI was also performed using a calibration coefficient obtained from 25 wt% montmorillonite samples, as shown in Equation 2, generating "Montmorillonite Adjusted Index" (MAI).

$$MAI = \frac{25\%}{mean\ MI\ for\ 25\,wt\%\,kaolinite\,samples} \cdot MI \quad (2)$$

Results and Discussion

Mineralogical characterization

The quantitative XRD analysis results of the samples are presented in Table 2. The tailings are primarily composed of feldspars (albite, orthoclase) and quartz, with smaller amounts of non-swelling phyllosilicates, such as muscovite and clinochlore. The kaolinite results show a significant amount of this pure phyllosilicate, along with a notable presence of K-feldspars (microcline and orthoclase) and amorphous material. For montmorillonite, the results do not indicate the presence of this phyllosilicate; instead, a substantial amount of amorphous material was observed. Additional characterization using reflectance spectroscopy was performed on kaolinite and montmorillonite briquettes to assess the XRD results obtained. The difference in reflectance values between the reference and measured spectra can be explained by grain size and mineral brightness in the VNIR-SWIR wavelength range, where smaller grain sizes result in higher SWIR reflectance.

Table 2: Quantitative XRD analysis.

	Specie	Chemical Formula	wt%
Kaolinite	Kaolinite 1A	$Al_2(Si_2O_5)(OH)_4$	68.01
	Microcline, intermediate	$KAlSi_3O_8$	8.14
	Orthoclase	$K_{.931}Na_{0.055}Ca_{.009}Ba_{.005}Al_{0.97}Si_{3.03}O_8$	8.02
	Muscovite 2M1	$K0.94Al_{1.96}(Al_{0.95}Si_{2.85}O_{10})((OH)_{1.744}F_{0.256})$	<0.5
	Quartz	SiO_2	4.37
	Tolbachite	$CuCl_2$	1.35
	AMORPHOUS	--------	9.93
Tailings	Quartz	SiO_2	31.3
	+Albite, Ca-rich, ordered	$(Na,Ca)Al(Si,Al)_3O_8$	40.56
	Orthoclase	$K_{.931}Na_{0.055}Ca_{.009}Ba_{.005}Al_{0.97}Si_{3.03}O_8$	6.93
	Muscovite-2M1	$KAl_2(Si_3Al)O_{10}(OH,F)_2$	12.77
	Clinochlore-1MIIb, Fe-rich	$(Mg,Fe)_6(Si,Al)_4O_{10}(OH)_8$	5.71
	Calcite	$Ca(CO_3)$	0.72
	Gypsum	$CaSO_4(H_2O)_2$	2.02
Montmorillonite	Muscovite 2M1	$(K_{0.82}Na_{0.18})(Fe_{0.03}Al_{1.97})(AlSi_3)O_{10}(OH)_2$	18.11
	Voltaite	$K_2Fe_5AlFe_3(SO_4)_{12}\cdot 18H_2O$	2.91
	Quartz, syn	SiO_2	2.71
	Alunogen	$(Al(H_2O)_6)_2(SO_4)_3(H_2O)_{4.4}$	13.34
	Vertumnite	$Ca_4Al_2(Si_{2.89}Al_{2.23}O_{5.18}(OH)_{21.88})(H_2O)_{4.38}$	0.20
	Amorphous	-------	62.75

The reflectance spectroscopy results for kaolinite and montmorillonite briquettes in the VNIR-SWIR wavelength range show a strong match with the reference spectra in TSG, as shown in Figures 2 & 3, this confirmed the large concentration of the corresponding phyllosilicate on reference samples. The montmorillonite used contained approximately 11.8% water under room conditions, so its natural humidity was considered as water addition for the experiments. Kaolinite was considered dry, as it did not exhibit any change after undergoing the same procedure described in Section 3.1. The measured densities for kaolinite, montmorillonite, and tailings were 2.5337, 2.9030, and 2.6721 g/cm^3, respectively, with the montmorillonite density adjusted to account for its natural humidity. Tailings combined with distilled water had a pH of 7, the same was obtained for pure kaolinite suspensions. In contrast, the pH of pure montmorillonite suspensions resulted between 1.8 and 2.0. Table 3 presents the particle size distribution of the samples obtained through laser diffraction. The results show that the kaolinite used in the experiments has a smaller particle size compared to montmorillonite, with d_{80} values of 13 and 56µm, respectively.

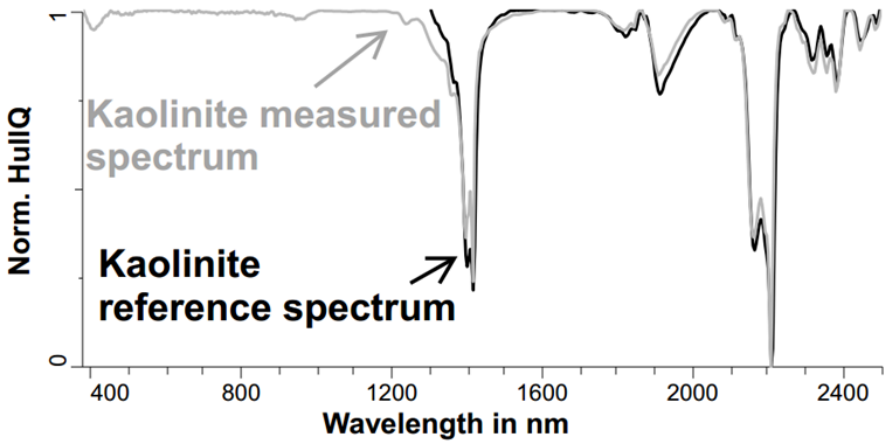

Figure 2: Kaolinite measured spectra from briquette and TSG reference. Hull quotient applied to reflectance spectra.

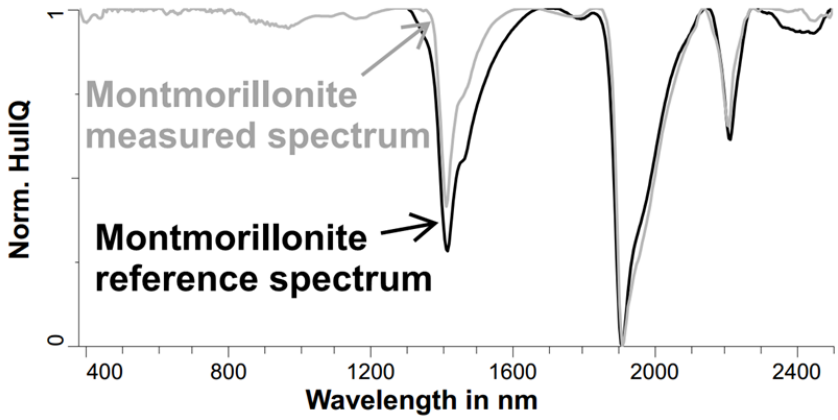

Figure 3: Montmorillonite measured spectra from briquette and TSG reference. Hull quotient applied to reflectance spectra.

Table 3: Particle size distribution of materials (Fu: Cumulative wt% passing).

Kaolinite			Montmorillonite			Tailings		
Microns	ASTM Mesh	Fu, %	Microns	ASTM Mesh	Fu, %	Microns	ASTM Mesh	Fu, %
425	40	99.99	425	40	99.99	425	40	99.84
300	50	99.99	300	50	99.99	300	50	99.12
212	70	99.99	212	70	99.99	212	70	95.96
150	100	99.99	150	100	99.91	150	100	88.56
106	140	99.99	106	140	96.62	106	140	77.89
75	200	99.99	75	200	87.17	75	200	66.74
53	270	99.99	53	270	77.08	53	270	59.82
45	325	99.63	45	325	61.51	45	325	52.4
38	400	98.98	38	400	51.53	38	400	48.11
<38	-400		<38	-400		<38	-400	

Rheometry results

Previous considerations: Three out of 108 total measurements were discarded due to anomalous behavior. Two of these exceeded the detection limit of the rheometer because of their high viscosity, while the third displayed unexpected noise in the measurement results. These three measurements were duplicated, but no reliable results were obtained; therefore, they were excluded from the data analysis.

Rheometer measurements at shear rates below $50s^{-1}$ were very noisy and unreliable due to the low shear stress of the suspensions in this range. As a result, the Bingham plastic model was fitted without including data points at low shear rates (typically less than $50s^{-1}$), using only the linear portion of the measured flow curves. This procedure may produce results that do not accurately represent the true behavior of the suspensions at low shear rates, such as in the gravitational discharge of tailings. The use of the Herschel-Bulkley model was evaluated, but excessive noise at low shear rates and unrealistic results-such as negative yield stress values-prevented the extraction of meaningful results when fitting the model.

Bingham viscosity and yield stress results: For each measurement, Bingham yield stress (τ_B) and Bingham viscosity (η_B) were obtained through the Bingham model adjustment, and the results were categorized based on the solids content by volume, particle size, phyllosilicate content in the solid phase, and the type of phyllosilicate used in the experiments. The results shown in Figure 4 indicate an exponential increase in yield stress and viscosity as the solid content by volume increases, which is consistent with previous study results [2,7,14].

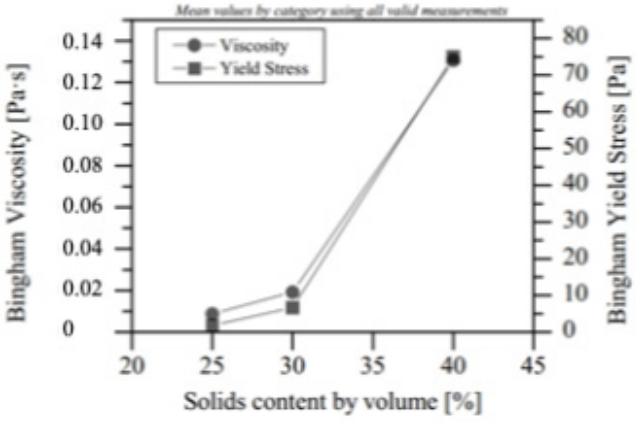

Figure 4: Viscosity and yield stress as a function of solid contents by volume.

An increase in phyllosilicate content in the solid phase also results in higher viscosity and yield stress, as shown in Figure 5. Yield stress appears to be more sensitive to this variable, with a variation of almost one order of magnitude between 5 and 25 wt%. A finer particle size also results in higher viscosity and yield stress, as depicted in Figure 6. The increase in these rheological properties when the solid phase is finer is well documented and has been described in previous studies [12,16,24,25].

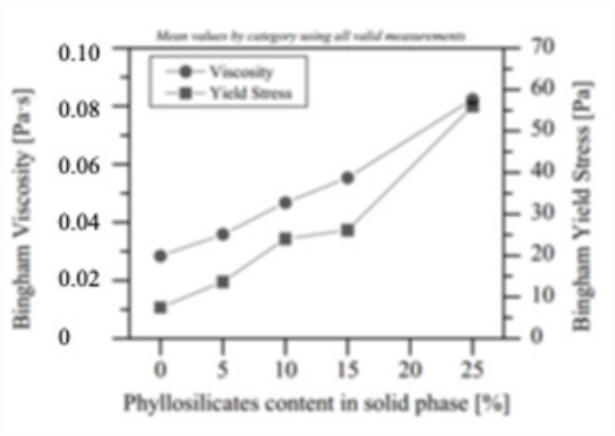

Figure 5: Viscosity and yield stress as a function of phyllosilicates content in solid phase.

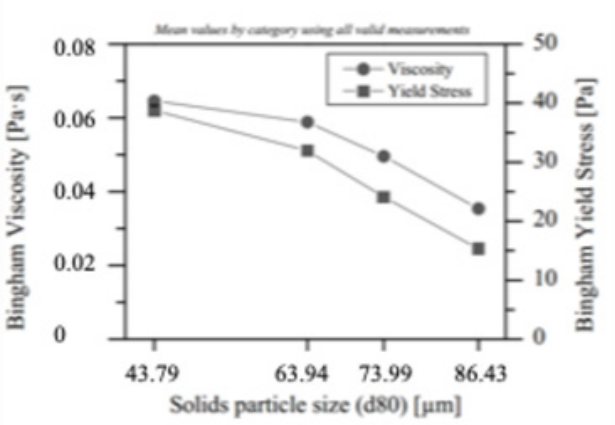

Figure 6: Viscosity and yield stress as a function of solid phase d_{80}.

The obtained results show that viscosity and yield stress are not dependent on the type of phyllosilicate, as shown in Figure 7. This can be attributed to the difference in particle size between the kaolinite (d_{80}=13µm) and montmorillonite (d_{80}=56µm) used in the experiments. Previous studies [10,14] have concluded that montmorillonite can have a greater capacity to increase viscosity and yield stress in suspensions due to its swelling behavior and high specific surface area, which can reach up to 100m^2g^{-1} in some cases [10].

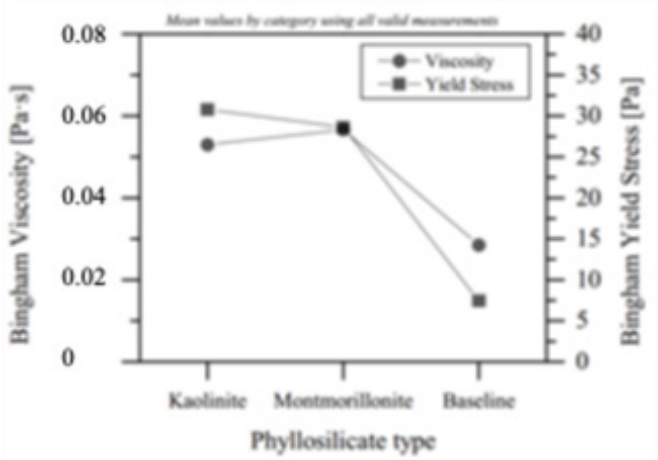

Figure 7: Viscosity and yield stress as a function of phyllosilicate type.

Linear regression models

Table 4 presents the results of both the normal and logarithmic approaches for linear regression. These results indicate that both models have at least one significant explanatory variable for yield stress and viscosity (ANOVA significance <5%). Additionally, it is evident that the logarithmic approach provides a better fit compared to the normal approach. This is due to the use of the Ordinary Least Squares (OLS) method for linear regression, which is highly sensitive to measured values that deviate significantly from the mean of the predicted variable. By applying the logarithmic transformation to the measured yield stress and viscosity, these differences are reduced, and the quality of the fit, as measured by the R^2 coefficient, is improved.

Table 4: Main results of linear regressions for both approaches. Regressions were performed using all valid (105) measurements.

Normal Approach	Tau Model				Eta Model			
	Coefficients	T Test Sig.	ANOVA Sig.	R^2	Coefficients	T Test Sig.	ANOVA Sig.	R^2
Constant	-118.660	.000			-.198	.000		
φ	524.893	.000			.867	.000		
d_{80}	-1.486	.784	.000	.551	.002	.682	0	.700
$wt\%_{phy}$	-0.640	.004			-.001	.001		
Phyllosilicate type	211.078	.000			.232	.000		
Logarithmic Approach	**Log Tau Model**				**Log Eta Model**			
	Coefficients	T Test Sig.	ANOVA Sig.	R^2	Coefficients	T Test Sig.	ANOVA Sig.	R^2
Constant	-2.219	.000			-3.884	.000		

φ	10.282	.000			7.658	.000		
d_{80}	-.009	.000	.000	.975	-.005	.000	0	.960
$wt\%_{phy}$	2.770	.000			1.348	.000		
Phyllosilicate type	.085	.000			.042	.011		

The normal approach indicates that particle size is not statistically significant at a 95% confidence level (T-test significance >5%) for predicting yield stress and viscosity, which contradicts established theory [19]. This issue does not arise in the logarithmic approach, making it both useful and consistent with the rheological results shown in Figure 6. Additionally, when comparing R^2 coefficients, the logarithmic approach provides better results than the normal one. For these reasons, the logarithmic approach was selected for further implementation with hyperspectral data. The model expressions obtained from the logarithmic approach are presented in Equations 3 and 4. Phyllosilicate type is treated as a categorical variable, with the following values: 1 for kaolinite, 2 for montmorillonite, and 0 for the baseline (suspensions without phyllosilicate doping).

$$Log\,\tau_{model} = 2.219 + 10.282\phi - 0.009d_{80} + 2.770wt\%_{phy} + 0.085\,phy.type \quad (3)$$

$$Log\,\eta_{model} = -3.884 + 7.658\phi - 0.005d_{80} + 1.348wt\%_{phy} + 0.042\,phy.type \quad (4)$$

SWIR reflectance spectra to estimate rheology

Solids content by volume (φ): Considering that reflectance spectroscopy was performed using solid dry briquettes, as previously described in section 3.4, the solids content by volume (φ) value had to be fixed manually in the obtained models.

Particle size (d_{80}) determination: The analysis of spectral features and mean reflectance quantification in the VNIR, SWIR, and TIR wavelength ranges was assessed as a possible method for determining particle size (d_{80}) in the briquettes. However, it was not possible to differentiate d_{80} between the samples using reflectance spectra. This is likely due to the narrow range of d_{80} values among the analyzed samples (43.79 to 86.43μm). Consequently, it can be concluded that SWIR spectra were not useful for particle size determination, and particle size had to be manually fixed in the yield stress and viscosity models.

Phyllosilicates differentiation: The differentiation criteria discussed in Section 3.6.1 were successfully implemented. Briquette samples prepared with kaolinite were clearly distinguished from those with montmorillonite and from the baseline samples. The values for the phyllosilicate type ("phy. type") variable were obtained through SWIR spectra and were used as input for the obtained models, based on the detected phyllosilicate.

Phyllosilicates quantification: The comparison between the experimental phyllosilicate contents in the briquettes and the values obtained from the kaolinite/montmorillonite index shows a good correlation, as indicated in Table 5. However, the Kaolinite Adjusted Index (KAI) seems to underestimate the kaolinite content in the samples, likely due to the index's calibration using samples with 25 wt% kaolinite. The Montmorillonite Adjusted Index shows a significant overestimation of montmorillonite content in the briquettes. This is primarily explained by the natural humidity of the montmorillonite, as well as the presence of OH-bearing minerals in the tailings, such as muscovite and clinochlore.

Table 5: Comparison of calculated and experimental mean values for kaolinite and montmorillonite amounts of phyllosilicates in briquettes.

Phyllosilicate Type	$wt\%_{phy}$	Adjusted Index %
Kaolinite	5	3.14
	10	8.03
	15	13.59
	25	25.00
Montmorillonite	5	9.18
	10	13.20
	15	17.00
	25	25.00

Model implementation: As mentioned previously, solids content by volume (φ) and particle size (d_{80}) were manually fixed in the models. In contrast, phyllosilicate content ($wt\%_{phy}$) and phyllosilicate type (phy. type) values were obtained using SWIR reflectance spectra. In several stages of copper extractive metallurgy, such as comminution, flotation, and thickening, φ and d_{80} are commonly controlled operational parameters. Therefore, their estimation via reflectance spectroscopy is not critical. However, phyllosilicate content and type are not regularly measured, making their estimation highly valuable for predicting the rheological behavior of pulps and tailings.

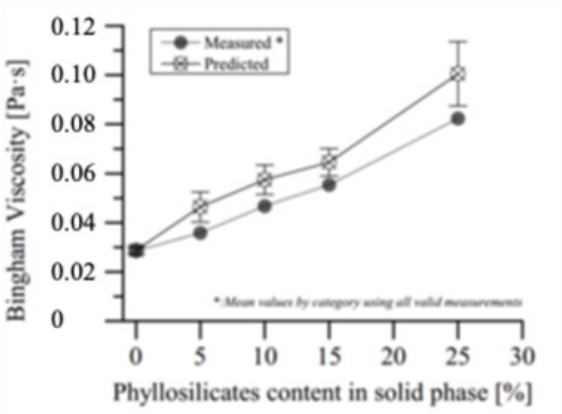

Figure 8: Measured and predicted viscosity for different phyllosilicates contents in solid phase.

The logarithm of yield stress and that of viscosity, obtained through the models using SWIR reflectance data, are referred to as $Log(\tau_{HL3})$ and $Log(\eta_{HL3})$, respectively. These values were then transformed back to predict yield stress (τ_{HL3}) and viscosity (η_{HL3}) and were compared with the measured Bingham yield stress

(τ_B) and Bingham viscosity (η_B), as shown in Table 6. Table 6 also indicates that the predicted viscosity (η_{HL3}) shows a better fit to the measured values than the predicted yield stress (τ_{HL3}). This is further confirmed by the results presented in Figure 8 & 9, where the predicted viscosity exhibits a lower mean absolute deviation (MAD; represented by error bars) compared to the predicted yield stress.

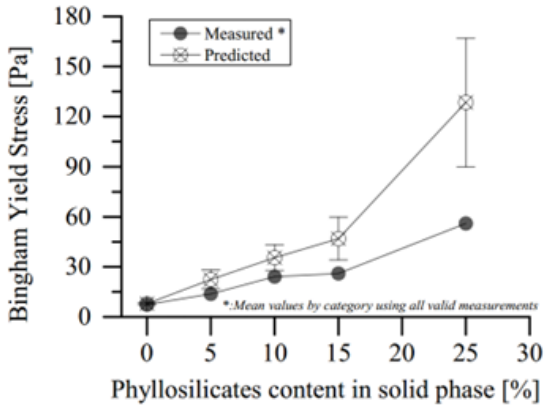

Figure 9: Measured and predicted yield stress for different phyllosilicates contents in solid phase.

Table 6: R^2 coefficients for predicted yield stress.

	$Log(\tau_{HL3})$	$Log(\eta_{HL3})$	τ_{HL3}	η_{HL3}
R^2	0.853	0.922	0.534	0.794

Table 7 shows that the Mean Absolute Percentage Error (MAPE) was particularly high for yield stress, sometimes exceeding 100%. These high MAD and MAPE values can be attributed to the overestimation of phyllosilicate content in the briquettes containing montmorillonite, which resulted in higher predicted yield stress and viscosity values in nearly all cases. The scatter plots shown in Figure 10 & 11 confirm that both predicted viscosity and yield stress, respectively, were overestimated. This overestimation is due to the values obtained from the "Montmorillonite Adjusted Index" scalar and the model's sensitivity to phyllosilicate abundance. The use of non-linear regression for viscosity and yield stress appears to be a key consideration for further model development. This approach could address the exponential growth of both rheological properties as solids content by volume increases.

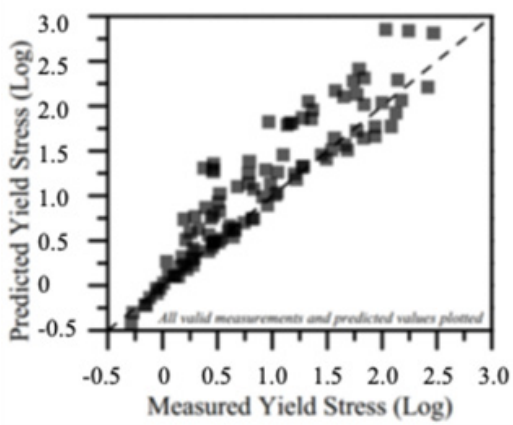

Figure 10: Logarithm of predicted and measured yield stress.

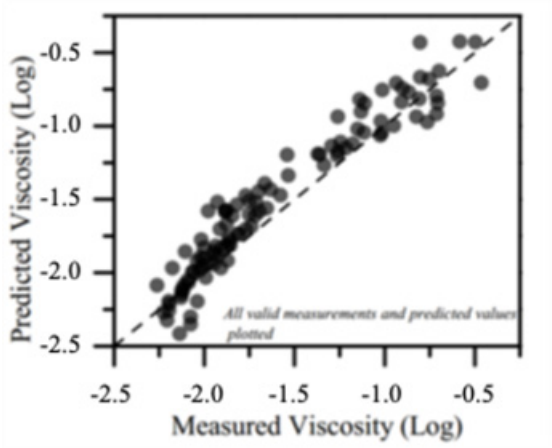

Figure 11: Logarithm of predicted and measured viscosity.

Table 7: Mean absolute deviation and mean absolute percentage error HyLogger3 model Mean values by category using all HyLogger3 predicted values.

Variable	Variables Values	η_{HL3}		τ_{HL3}	
		MAD[Pa·s]	MAPE [%]	MAD [Pa]	MAPE [%]
Solids Content by Volume [%]	25	0.001	11.37	1.04	57.08
	30	0.002	10.38	3.07	45.73
	40	0.011	8.45	27.95	37.25
Phyllosilicates Content in Solid Phase [%]	0	0.001	5.24	0.46	6.12
	5	0.006	17.17	5.66	41.26
	10	0.006	12.83	7.71	32.05
	15	0.006	10.04	12.84	49.23
	25	0.013	15.77	38.49	68.83
Particle Size [µm]	86.43	0.010	26.95	23.34	152.55
	73.99	0.005	10.55	20.20	83.85
	63.94	0.005	7.88	16.14	50.55
	43.79	0.009	13.69	7.44	19.19

Phyllosilicate Type	Kaolinite	0.004	7.73	3.11	10.11
	Montmorillonite	0.007	12.89	21.01	73.34
	Base Line	0.001	5.24	0.46	6.12

A better fit for predicted viscosity (η_{HL3}) and yield stress (τ_{HL3}) may also be achievable by applying a different mathematical treatment to the spectral features of kaolinite and montmorillonite, particularly for the latter, given its shared characteristics with other OH-bearing minerals [26,27].

Conclusion

This study developed an empirical model to estimate the viscosity (η) and yield stress (τ) of copper tailings containing phyllosilicates (montmorillonite and kaolinite), based on rheological experiments and data obtained from advanced characterization techniques, including hyperspectral analysis, X-Ray Fluorescence (XRF), X-Ray Diffraction (XRD), and laser diffraction particle sizing, applied to various industrial samples. Four key rheological variables were considered: solids content by volume (φ), particle size (d_{80}), phyllosilicate content in the solid phase ($wt\%_{phy}$), and phyllosilicate type (phy. type). The resulting linear model demonstrated a good fit (R^2>0.85), confirming that φ is the most dominant factor, followed by wt%phy. Incorporating rheological models, such as the Herschel-Bulkley model, would be beneficial for predicting the behavior of suspensions at low shear rates. However, the primary requirement for this is the acquisition of reliable shear stress measurements under such conditions.

The results demonstrated that the advanced characterization techniques used in this study complement one another effectively for estimating the yield stress and viscosity of phyllosilicate-rich tailings. This was particularly evident in the spectral measurements using hyperspectral HyLogger3 and TSGTH software on montmorillonite, which enabled the identification of this mineral even when quantitative XRD results were inconclusive. This research confirms that hyperspectral analysis is a valuable tool for generating preliminary estimations of viscosity and yield stress, especially given that solids content by volume and particle size are commonly controlled operational parameters in the industry. However, improving the accuracy of phyllosilicate content estimation is necessary for a more reliable rheology prediction system, as the models are highly sensitive to the quantitative presence of these minerals.

References

1. Lin Y, Qin H, Guo J, Chen J (2021) Study on the rheological behavior of a model clay sediment. J Mar Sci Eng 9(1): 81.
2. Becker M, Yorath G, Ndlovu B, Harris M, Deglon D, et al. (2013) A rheological investigation of the behaviour of two Southern African platinum ores. Miner Eng 49: 92-97.
3. Bulatovic S, Wyslouzil D, Kant C (1999) Effect of clay slimes on copper, molybdenum flotation from porphyry ores. Proc Copp.
4. de Kretser R, Scales PJ, Boger DV (1997) Improving clay-based tailings disposal: Case study on coal tailings. AIChE J 43(7): 1894-1903.
5. Kwak M, James DF, Klein KA (2005) Flow behaviour of tailings paste for surface disposal. Int J Miner Process 77(3): 139-153.
6. McFarlane AJ, Addai-Mensah J, Bremmell K (2005) Rheology of flocculated kaolinite dispersions. Korea-Australia Rheol J 17: 181-190.
7. Ndlovu B, Farrokhpay S, Bradshaw D (2013) The effect of phyllosilicate minerals on mineral processing industry. Int J Miner Process 125: 149-156.
8. Nosrati A, Addai-Mensah J, Skinner W (2012) Muscovite clay mineral particle interactions in aqueous media. Powder Technol 219: 228-238.
9. Alejo B, Barrientos A (2009) Model for yield stress of quartz pulps and copper tailings. Int J Miner Process 93(3-4): 213-219.
10. Ayadi A, Soro J, Kamoun A, Baklouti S (2013) Study of clay's mineralogy effect on rheological behavior of ceramic suspensions using an experimental design. Int J Mat Sci 14: 374-384.
11. Whitbourn L, Huntington J, Munday T (2011) CSIRO' s hyLogging TM systems–Production proven technology for the exploration and mining sector. Explor Technol, pp. 85-88.
12. Blakey BC, James DF (2003) Characterizing the rheology of laterite slurries. Int J Miner Process 70(1-4): 23-39.
13. de Kretser RG, Scales PJ, Boger DV (1998) Surface chemistry-rheology inter-relationships in clay suspensions. Colloids Surfaces A Physicochem Eng Asp 137(1-3): 307-318.
14. Ndlovu B, Forbes E, Farrokhpay S, Becker M, Bradshaw D, et al. (2014) A preliminary rheological classification of phyllosilicate group minerals. Miner Eng 55: 190-200.
15. Ndlovu B, Becker M, Forbes E, Deglon D, Franzidis JP (2011) The influence of phyllosilicate mineralogy on the rheology of mineral slurries. Miner Eng 24(12): 1314-1322.
16. Tangsathitkulchai C, Austin LG (1988) Rheology of concentrated slurries of particles of natural size distribution produced by grinding. Powder Technol 56(4): 293-299.
17. Tangsathitkulchai C (2003) The effect of slurry rheology on fine grinding in a laboratory ball mill. Int J Miner Process 69(1-4): 29-47.
18. Yang HG, Li CZ, Gu HC, Fang TN (2001) Rheological behavior of titanium dioxide suspensions. J Colloid Interface Sci 236(1): 96-103.
19. Barnes H, Hutton J, Walters K (1989) An introduction to rheology.
20. Madsen FT, Muller-Vonmoos M (1989) The swelling behaviour of clays. Applied Clay Science 4(2): 143-156.
21. Mason P, Huntington J (2012) HyLogger 3 components and pre-processing: An overview. Northern Territory Geological Survey, Technical Note 2012-002, Australia.
22. Cooper CD, Mustard JF (1999) Effects of very fine particle size on reflectance spectra of smectite and palagonitic soil. Icarus 142(2): 557-570.
23. Myers TL, Brauer CS, Su FY, Blake TA, Tonkyn RG, et al. (2015) Quantitative reflectance spectra of solid powders as a function of particle size. Appl Opt 54(15): 4863-4875.
24. He M, Wang Y, Forssberg E (2004) Slurry rheology in wet ultrafine grinding of industrial minerals: A review. Powder Technol 147(1-3): 94-112.

25. Logos C, Nguyen QD (1996) Effect of particle size on the flow properties of a South Australian coal-water slurry. Powder Technol 88(1): 55-58.

26. Fisher DT, Clayton SA, Boger DV, Scales PJ (2007) The bucket rheometer for shear stress-shear rate measurement of industrial suspensions. J Rheol 51(5): 821-831.

27. Stickland AD, Kumar A, Kusuma TE, Scales PJ, Tindley A, et al. (2015) The effect of premature wall yield on creep testing of strongly flocculated suspensions. Rheol Acta 54: 337-352.